Sulfur Isotope Evidence for Microbial Sulfate Reduction in Altered Oceanic Basalts at ODP Site 801

Olivier Rouxel [1,*], Shuhei Ono [2,#], Jeff Alt [3], Douglas Rumble [2]
and John Ludden [4,5]

[1] Marine Chemistry & Geochemistry Department, Woods Hole Oceanographic Institution, MS #25, Woods Hole MA 02543

[2] Geophysical Laboratory, Carnegie Institution of Washington, 5251 Broad Branch Rd. NW, Washington DC 20015

[3] Department of Geological Sciences, The University of Michigan, Ann Arbor, MI 48109

[4] Centre de Recherches Pétrographiques et Géochimiques, CNRS UPR 2300, BP 20, 54501 Vandoeuvre-les-Nancy cedex, France

[5] British Geological Survey, Keyworth, Nottingham, NG12 5GG, UK

* Corresponding author:

Olivier Rouxel (email: orouxel@whoi.edu; phone: 508-289-3655; fax: 508-457-2193)

 # Present Address:

Department of Earth, Atmospheric, and Planetary Sciences, Massachusetts Institute of Technology, 77 Massachusetts Avenue, Cambridge, MA 02139

Keyword: sulfur isotopes, seafloor weathering, deep biosphere, oceanic crust, sulfur cycle

ABSTRACT

The subsurface biosphere in the basaltic ocean crust is potentially of major importance in affecting chemical exchange between the ocean and lithosphere. Alteration of the oceanic crust commonly yields secondary pyrite that are depleted in ^{34}S relative to igneous sulfides. Although these ^{34}S depleted sulfur isotope ratios may point to signatures of biological fractionation, previous interpretations of sulfur isotope fractionation in altered volcanic rocks have relied on abiotic fractionation processes between intermediate sulfur species formed during basalt alteration. Here, we report results for multiple-S isotope (^{32}S,^{33}S,^{34}S) compositions of altered basalts at ODP Site 801 in the western Pacific and provide evidence for microbial sulfate reduction within the volcanic oceanic crust. *In-situ* ion-microprobe analyses of secondary pyrite in basement rocks show a large range of $\delta^{34}S$ values, between –45‰ and 1‰, whereas bulk rock $\delta^{34}S$ analyses yield a more restricted range of –15.8 to 0.9‰. These low and variable $\delta^{34}S$ values, together with bulk rock S concentrations ranging from 0.02% up to 1.28% are consistent with loss of magmatic primary mono-sulfide and addition of secondary sulfide via microbial sulfate reduction. High-precision multiple-sulfur isotope ($^{32}S/^{33}S/^{34}S$) analyses suggest that secondary sulfides exhibit mass-dependent equilibrium fractionation relative to seawater sulfate in both $\delta^{33}S$ and $\delta^{34}S$ values. These relationships are explained by bacterial sulfate reduction proceeding at very low metabolic rates. The determination of the S-isotope composition of bulk altered oceanic crust demonstrates that S-based metabolic activity of subsurface life in

oceanic basalt is widespread, and can affect the global S budget at the crust-seawater interface.

1. Introduction

Alteration of oceanic crust by seawater is one of the most important processes controlling the global fluxes of many elements (e.g. Staudigel and Hart, 1983) and microbes likely play a significant role in this process (Bach and Edwards, 2003). The evidence for a deep biosphere within oceanic basement includes primarily the alteration textures of volcanic glass, the potential presence of DNA or high C, N and P contents in altered glass, and the light isotopic composition of C in some carbonate veins (e.g. Thorseth et al., 1992; Fisk et al., 1998; Furnes et al., 2001). However, the study of an active biosphere in the basaltic ocean crust is currently limited and lags behind our current understanding of subsurface life in deep-sea sediments (Parkes et al., 1994; Wortmann et al., 2001; D'Hondt et al., 2002). This is mainly due to technical difficulties involved in identifying and culturing indigenous microbes, as well as the lack of a visual record of microbial activity in crystalline rocks in contrast to volcanic glass.

Previous studies of sulfur isotope compositions of deep sea sediments have shown that sulfate-reducing communities are active in the deeply buried sediments and that their cellular metabolic activities may differ from those observed in near-surface sediments or in the water column (Wortmann et al., 2001). Sulfur isotope values of secondary pyrite precipitated in oceanic basalt fractures have been reported in numerous studies (Field et al., 1976; Krouse et al., 1977; Andrews, 1979; Puchelt et al., 1996) and $\delta^{34}S$ values generally range from basaltic values at 0‰ to highly negative values down to -50‰. Although these negative $\delta^{34}S$ values are consistent with an origin involving microbial reduction of seawater sulfate, as commonly observed in marine sediment settings (Canfield, 2002), previous

researchers favored an abiotic isotope fractionation process due to the lack of a well-identified organic carbon source in the basalts (Field et al., 1976; Andrews, 1979; Puchelt et al., 1996). In a previous model, Andrews (1979) proposed that igneous sulfide minerals are partially oxidized to unstable intermediate sulfur species (e.g. sulfite, SO_3^{2-}, or thiosulfate, $S_2O_3^{2-}$) which can inorganically disproportionate into sulfate and sulfide. Sulfate is lost from the rock, whereas sulfide, which combines with iron in the host rock, is precipitated as secondary pyrite. Recently, elevated $\delta^{34}S$ values (26.2 to 29‰) of preserved gypsum in exposed ophiolitic oceanic crust have been interpreted as the result of *in-situ* microbial sulfate reduction (Alt et al., 2003) but questions remain concerning the origin (i.e. abiotic or biotic), mechanisms (i.e. sulfate reduction or disproportionation), and global significance of the low $\delta^{34}S$ values in secondary sulfides in altered basalts.

Drilling at Ocean Drilling Program (ODP) Site 801 penetrated more than 400m into Jurassic oceanic basement in the western Pacific (Larson et al., 1992; Plank et al., 2000). This section represents the oldest *in-situ* oceanic basement ever drilled and presents an excellent opportunity to explore potential S-isotope biosignatures of the deep biosphere. In this paper, we use three S isotope approaches to unravel the mechanisms of S-isotope fractionation associated with the alteration of the oceanic crust at ODP Site 801. First, *in-situ* ion microprobe $\delta^{34}S$ analyses were undertaken to document isotopic heterogeneity and textural relationship for secondary sulfides in altered rocks and veins. Second, analyses of multiple S-isotopes ($^{32}S/^{33}S/^{34}S$) for selected secondary sulfides in the altered basalts were used to constrain multiple-sulfur isotope relationships between primordial sulfur and seawater sulfate. Analysis of $\delta^{33}S$ combined with standard $\delta^{34}S$ analysis provides a new

dimension in documenting reactions involving sulfur, such as reaction pathways during microbial sulfate reduction and S-disproportionation (Farquhar et al., 2003; Johnston et al., 2005; Ono et al., 2006). Finally, bulk rock S-isotope analyses are used to assess the large-scale budget of sulfur isotopes in altered oceanic basement at ODP Site 801.

2. Geological setting and alteration history

ODP Site 801 is located in the Pacific plate several hundred kilometers east of the Marianas trench (**Fig.1**). ODP Site 801 was drilled into Jurassic basement characterized by a lack of magnetic anomalies and a half-spreading rate of about 8 cm/yr (Larson et al., 1992; Plank et al., 2000). On the basis of flow morphology, geochemistry, and mineralogy, the basement section at Hole 801C, which was intersected at 461.6 meters below seafloor (mbsf), has been divided into four major sequences which include rocks drilled on both Leg 129 and Leg 185 (Larson et al., 1992; Plank et al., 2000; Kelley et al., 2003) (**Fig. 2**).

The uppermost basement (Unit ALK) is composed of alkaline basaltic to dolerite sills overlying a Si and Fe oxyhdroxide-rich hydrothermal horizon (H.D. in **Fig.2**). The alkali basalt section is younger (157 Ma; Pringle, 1992; Koppers et al., 2003) than the underlying tholeiitic mid-ocean ridge basalt (MORB) section (~170 Ma). Below the hydrothermal deposit, the volcanic rocks (Unit MORB 0-110) comprise thin flows and pillows, lying above a series of thick lava flows. The upper 110 m of MORB (MORB 0-110 of **Fig.1**) are thought to have erupted slightly off-axis (Pockalny and Larson, 2003). The on-axis MORB is divided into a middle (MORB 110-220) and a lower (MORB 220-420) unit, distinguished on the basis of a change in eruptive styles, with more massive flows in the lower unit. Between 600 and 720 mbsf the section is characterised by a pillow-

dominated zone with a well-developed interpillow horizon (Unit MORB 110-220). A second Si-Fe-rich hydrothermal unit similar to the larger one uphole is present within Unit MORB 110-220 pillows (**Fig. 2**). From 720 mbsf to the bottom at 936 mbsf, the Unit MORB 220-420 comprises a tectonic breccia which separates a massive flow unit (720-890 mbsf) and a series of thin, generally <1-m-thick, sheet flows and pillows (890-934 mbsf).

Three general types of low temperature alteration can be observed (Alt and Burdett, 1992; Plank et al., 2000; Talbi and Honnorez, 2003): (1) replacement of igneous material in alteration halos and groundmass; (2) filling of void space by secondary phases; (3) development of breccia cements and cross-cutting veins. The latter are often filled with calcite, and can reopen and refill for millions of years, providing an important sink for carbon in the altered crust (Alt and Teagle, 1999). The most common secondary phases are saponite (Mg-smectite), calcite, celadonite, Fe-oxyhydroxide and pyrite (Alt and Teagle, 2003; Talbi and Honnorez, 2003). Most of the basalts are dark gray in color and have experienced 10 to 20% alteration (Alt and Teagle, 2003). In addition, both dark celadonite-rich, and brown Fe-oxyhydroxide alteration halos around fractures are observed. Secondary pyrite generally occurs within saponite-rich and carbonate veins but is also found at the boundary between the alteration halos and the host rock. Alteration of basalts at Site 801 took place at low temperatures (<100˚C), mainly off-axis, during aging of the oceanic crust (Plank et al., 2000; Alt and Teagle, 2003; Talbi and Honnorez, 2003). Fresh basaltic glass is locally preserved at Site 801C, demonstrating the heterogeneous distribution of low temperature alteration. Volcanic glass recovered throughout the section is altered by invasive channels and tubes which are similar to other examples in basaltic glass in the deep ocean crust that have been attributed to microbial alteration (Plank et al., 2000).

3. Methodology

3.1 Sampling strategy

A comprehensive set of samples, covering the major Units at Site 801, were selected for this study (**Table 1**). All of the selected rocks have been affected by low temperature alteration (< 100°C) resulting in various combinations of secondary minerals saponite (Mg-smectite), calcite, celadonite, Fe-oxyhydroxide and pyrite as replacements of igneous phases and as fillings of vesicles and cracks. A subset of samples was also selected for *in-situ* S-isotope analysis based on the occurrence of macroscopic pyrite along veins and disseminated in the groundmass (**Table 2**).

We analyzed one composite sample (referred as SUPER) which represents a physical mixture of a subset of individual samples covering all basement lithologies identified at site 801C (Plank et al., 2000; Revillon et al., 2002; Kelley et al., 2003). This SUPER composite was prepared by making a proportionate mixture of sub-composites (volcanic flows and volcanoclastites) from each of the three MORB intervals. These sub-composites were themselves prepared from 117 representative samples from each core segments from the basement section of Hole 801C (Kelley et al., 2003). Though detailed information about fine-scale variations can be obtained only from the analysis of individual samples, the use of composites allows to estimate the average composition with very few analyses. Hence, we used S concentration and S-isotope composition of the SUPER composite to approximate the large-scale composition of the entire MORB section at Site 801.

137

138 *3.2. S-isotope definitions and notations*

139 Sulfur isotope values are reported using conventional delta notation:

140 $$\delta^{x}\mathrm{S} = \left(\frac{{}^{x}R_{\mathrm{sample}}}{{}^{x}R_{\mathrm{reference}}} - 1 \right) \times 1{,}000 \quad (‰) \tag{1}$$

141 where ${}^{x}R$ is the isotope ratio, ${}^{x}\mathrm{S}/{}^{32}\mathrm{S}$ (x=33 or 34), of the sample compared to reference
142 material. S-isotope data are reported on the Vienna-CDT scale (VCDT) by defining $\delta^{33}\mathrm{S}$
143 and $\delta^{34}\mathrm{S}$ of IAEA S-1 (artificial Ag_2S) to be –0.055 and –0.300‰, respectively (Coplen
144 and Krouse, 1998; Ono et al., 2007).

145 We define *traditional* capital delta notation (Δ) as deviations of $\delta^{33}\mathrm{S}$ from a reference
146 line :

147 $$\Delta^{33}\mathrm{S} = \delta^{33}\mathrm{S} - 0.515 \times \delta^{34}\mathrm{S} \tag{2}$$

148 An alternative Δ definition has been preferred by recent studies (Hulston and Thode, 1965;
149 Gao and Thiemens, 1991; Miller, 2002; Young et al., 2002), and we denote this as Δ*:

150 $$\Delta^{33}\mathrm{S}^{*} = \delta^{33}\mathrm{S}^{*} - 0.515 \times \delta^{34}\mathrm{S}^{*} \tag{3}$$

151 where

152 $$\delta^{x}\mathrm{S}^{*} = \ln\left(\frac{{}^{x}R_{sample}}{{}^{x}R_{ref}} \right) \times 1{,}000 = \ln\left(\frac{\delta^{x}\mathrm{S}}{1{,}000} + 1 \right) \times 1{,}000 \tag{4}$$

153 Both definitions (Δ and Δ*) are used in **Table 3** for comparison. Note that the
154 modified delta notations ($\delta^{34}\mathrm{S}^{*}$ and $\Delta^{33}\mathrm{S}^{*}$) are *fractionation-oriented* (i.e. linear
155 relationships during mass-dependent isotope fractionation) whereas traditional delta

156 coordinates ($\delta^{34}S$ and $\Delta^{33}S$) are *mass-balance oriented* (i.e. linear relationships during
157 mixing) (Ono et al., 2007).

158 Mass-dependent sulfur isotope fractionation factors are described by the following
159 power law (Hulston and Thode, 1965; Farquhar et al., 2003; Ono et al., 2007) :

160 $$^{33}\alpha = {}^{34}\alpha^{\,^{33}\theta} \quad (5)$$

161 where fractionation factors ($^{x}\alpha$) are defined as the ratio of $^{x}S/^{32}S$ between two pools of
162 sulfur (e.g., A and B). That is,

163 $$^{x}\alpha = (^{x}S/^{32}S)_A/(^{x}S/^{32}S)_B \quad (6)$$

164 The $^{33}\theta$ value for equilibrium isotope fractionation factors between SO_4^{2-} and H_2S
165 may also vary as a function of temperature, from 0.5145 at 0°C to 0.5154 at 500°C (Ono et
166 al., 2007) while microbial sulfate reduction follows different $^{33}\theta$ value of ~ 0.512 (Farquhar
167 et al., 2003; Ono et al., 2007).

168

169 *3.3. Bulk rock analysis:*

170 Solid sample surfaces were cleaned with a sand-blaster and washed with distilled
171 water. Sample powders for bulk rock analysis were prepared using agate grinding vessels.
172 Major element chemistry was determined by ICP-AES at CRPG-CNRS (France) following
173 the procedure described in Govindaraju and Mevelle (1987) and results are presented in
174 **Table 1**. S concentrations were analyzed in 250 mg bulk rock samples using a
175 LECO144DR carbon-sulfur analyzer. The precision is estimated at 5% for S content
176 >0.05% and the limit of detection is 0.005%.

177 Sulfur isotope compositions of bulk rocks were determined following the procedure
178 of Rice et al. (1993) and Canfield et al. (1986) and data are reported in **Table 1**. Acid-
179 volatile sulfides (AVS) were first extracted in HCl with $SnCl_2$ added to prevent oxidation.
180 Chromium-reducible sulfides (Cr-S) were subsequently extracted using the Cr-reduction
181 method (**Table 1**). Evolved H_2S for AVS and Cr-S were precipitated as Ag_2S, and acid
182 soluble sulfate was reduced to H_2S with Thode's solution and precipitated as Ag_2S. Sulfur
183 isotope analyses of Ag_2S were performed at Queen's University (Canada). Yields from the
184 sulfur extractions average 90% of the bulk S concentrations from LECO C-S analyzer, but
185 only the latter are reported. Total $\delta^{34}S$ composition is obtained by mass balance calculation
186 between AVS and Cr-S.
187
188 *3.4. Micro-drilled sulfide analysis:*
189 The $^{34}S/^{32}S$ analyses of micro-drilled sulfides (**Table 2**) were performed on a
190 VG602D double-collector mass spectrometer at CRPG and are given in conventional $\delta^{34}S$
191 notation relative to V-CDT (Coplen and Krouse, 1998). We used the NIST sulfide standard
192 NZ-1 defined at -0.3‰ and we obtained NZ-2= 21.6‰ ± 0.1‰, NZ-3= -31.6‰ ± 0.1‰,
193 NBS-123= 17.4‰ ± 0.1‰, NBS-127= 20.4‰ ± 0.2‰ based on replicate measurements.
194 The precision for sulfide data is typically ± 0.2‰ (2 sigma level) and is often better than
195 0.1‰.
196 The $^{34}S/^{32}S$ and $^{33}S/^{32}S$ analyses were performed at the Carnegie Institution of
197 Washington (USA). The fluorination manifold is coupled on-line with a two-stage gas
198 chromatography purification system, which is critical for ultra-high precision isotope ratios

measurements. Multiple sulfur isotope ratios are analyzed by a gas-source mass-spectrometer (Finnigan MAT 253) with SF_6 as analyte. Details of the analytical technique can be found in Hu et al. (2003) and Ono et al. (2006). For isotope analysis, Ag_2S (~ 1.5 mg) were prepared by conventional distillation (Cr-reduction) after precise micro-drilling of rock matrix containing large sulfide grains in polished section (**Supplementary Materials**). Precision and accuracy are 0.2 and 0.004 ‰ for $\delta^{34}S$ and $\Delta^{33}S$, respectively (Ono et al., 2006). Isotope results are reported in **Table 3**.

3.5. Ion-microprobe analysis:

S isotope compositions of pyrite and marcasite, ranging in size from 100 μm up to 2 mm in diameter, hosted in the basalt groundmass or occurring within vein fractures (**Table 2** and **Fig. 2**) were determined using a modified CAMECA IMS 3F ion microprobe at the CRPG (Chaussidon and Demange, 1988). Rock chips were mounted in epoxy together with an internal pyrite S-isotope standard (GAV18), polished, and coated with gold. Sulfides were sputtered with a 10-15 nA O^- primary beam of 50μm in diameter. Secondary $^{32}S^+$ and $^{34}S^+$ ions were analyzed in mono-collector mode without energy filtering at a mass resolution of 3000 as no sulfur hydrides were observed. The instrumental mass fractionation (the difference between $\delta^{34}S$ obtained with the ion probe and the true value) was determined at -47‰ using the internal standard GAV18 defined at 10.5‰ relative to V-CDT. Under normal conditions, the internal precision of S-isotope analysis is about 1.0‰. However, during the analytical period of this study, reproducibility of the standard measured between each sample data point in the same polished section was somewhat

poorer (2.0 ‰ at 95% confidence level for 40 analyses). This is mainly due to instability of the primary gun and/or change of instrumental bias during repositioning of the sample.

4. Results and Discussion

4.1. ^{34}S - ^{32}S isotope profile through basaltic oceanic crust section

S-isotope analyses of bulk basalt and individual Fe-sulfide grains (pyrite and marcasite) display a large spread of $\delta^{34}S$ values from 1.3‰ down to –45‰ (**Fig.2**). *In situ* ion-microprobe analyses reveal that $\delta^{34}S$ values lower than –20‰ (e.g. sample 801B-43R1,29; 801C-39R2,28) are commonly found in pyrite and marcasite precipitated in open space of altered basalts, such as within mm-thick carbonate veins, thin fractures lined with saponite or in vesicles (**Fig.3**). In contrast, $\delta^{34}S$ values higher than –10‰ (e.g. sample 801C-24R2,36; 801C-37R1,83) are preferentially found for secondary sulfides disseminated within the basalt matrix. Although significant isotopic variations of up to 10‰ occur at sub-mm scales, showing the existence of several generations of sulfide minerals having distinct S-isotope compositions (**Fig.3**), no systematic $\delta^{34}S$ zonation within sulfide grains could be identified. As evident from **Figure 2**, no clear trend can be drawn along the depth profile and highly negative $\delta^{34}S$ values analyzed by ion microprobe are found at the greatest depth (840 mbsf). As expected, S isotope compositions of bulk rocks do not display the same degree of variability as for *in situ* analysis and $\delta^{34}S$ values for both AVS and Cr-S vary between 0.9 and –15.8‰. In general, AVS yields higher $\delta^{34}S$ values than Cr-S by up to 5‰, although some samples (e.g. 801C-37R1,83) display inverse

243 relationships. Less negative $\delta^{34}S$ values for AVS are explained by considering that AVS
244 fraction preferentially sampled primary pyrrhotite having primordial isotope compositions
245 ($\delta^{34}S \approx 0‰$). The SUPER composite yields negative $\delta^{34}S$ values of –2.7‰ for AVS and –
246 8.4‰ for Cr-S, with the bulk sulfide-S (i.e., AVS + Cr-S) of the uppermost 440 m of
247 volcanic basement at Site 801 having $\delta^{34}S = –6.8‰$.

248 Altered basalts at Site 801 are generally characterized by heterogeneous S
249 concentrations (**Table 1**) ranging from values lower than 0.02% to values up to 1.28%.
250 Based on electron microprobe analyses of fresh volcanic glass recovered through the 801C
251 tholeiitic section, primary magmatic S contents are estimated, on average, to be 0.21±0.06
252 wt% (Fisk and Kelley, 2002). Since magma degassing at the seafloor leads to loss of, on
253 average, one third of the sulfur in the melt (Moore and Fabbi, 1971), S concentration of the
254 fresh crystalline 801C basalt section is estimated between 0.17 and 0.12 wt%. Bulk rock
255 analysis of altered basalts at ODP Site 801 (**Table 1**) reveal that some intervals may display
256 S-enrichment relative to fresh basalts (S up to 1.30%, sample 801C-37R5,30) and negative
257 $\delta^{34}S$ values (-12.9‰). These discrete intervals are best explained by a net addition of
258 secondary sulfide having negative $\delta^{34}S$. It should be also noted that S-depleted altered
259 basalt, such as sample (801C-15R4,69) may also display minimal S-isotope fractionation,
260 suggesting that sulfide oxidation may proceed without significant S-isotope fractionation.

261 An important question to address is whether these low and highly variable $\delta^{34}S$
262 values and S-enrichment through the basaltic oceanic crust section at ODP Site 801 result
263 from the downward diffusion (or advection) of H_2S from overlying sediment section or
264 result from *in-situ* S-isotope fractionation. Sediments at Site 801 are mostly oxidized

265 pelagic sediments, composed of chert, porcellanite and volcaniclastic turbidites with very
266 little organic carbon (Alt and Burdett, 1992). As a consequence, sulfate reduction is limited
267 throughout the overlying sediment section at ODP Site 801, as demonstrated by porewater
268 sulfate concentrations above 16mM and the lack of detectable level of dissolved sulfide in
269 porewaters (Alt and Burdett, 1992). In addition, the thick chert and porcellanite Units at
270 801 provide a low-permeability barrier to vertical diffusion between upper sediments and
271 deeper volcaniclastic turbidites. These layers would have prevented diffusion of H_2S and
272 nutrients into the basement from any organic rich sediments deposited in the high-
273 productivity equatorial upwelling zone at about 90-80 Ma (Alt and Burdett, 1992).

274 The fact that sedimentary pyrite at ODP Site 801 yields less negative $\delta^{34}S$ values
275 (between -14 to -21‰, Alt and Burdett, 1992) than for secondary pyrite in the underlying
276 altered basement, together with the lack of a systematic downhole trend in $\delta^{34}S$ values
277 along the volcanic section (**Fig. 2**) suggest an *in-situ* sulfate reduction origin for secondary
278 sulfide in the volcanic basement at Site 801. In fact, the large heterogeneity of $\delta^{34}S$ values
279 for secondary pyrite within individual samples (e.g. sample 801C-17R1,100; Table 2) is
280 better explained by *in-situ* S-isotope fractionation within basement rather than sedimentary
281 origin. Low $\delta^{34}S$ values of pyrite and marcasite in open space (veins) between – 35 to – 45
282 ‰ are thus consistent with open-system bacterial sulfate reduction under unlimited sulfate
283 supply. In contrast, higher $\delta^{34}S$ values up to 0‰ could reflect either closed-system bacterial
284 sulfate reduction or mixing between biogenic and igneous (i.e. unfractionated) sulfides.

285 It remains unclear, however, whether these highly negative $\delta^{34}S$ values down to –45
286 ‰ are generated by (1) abiotic fractionation during sulfide partial oxidation and

reprecipitation, as suggested previously by Andrews (1979); (2) single-step bacterial sulfate reduction, as suggested from deep marine sediments porewater studies (Wortmann et al., 2001); (3) bacterial disproportionation of intermediate S-species, as commonly proposed for sedimentary sulfides (Canfield and Thamdrup, 1994). Comparisons between $\delta^{34}S$ values and S concentrations of altered basalts as well as multiple S-isotope systematics may help in solving these issues as described below.

4.2. Mechanisms of S loss and uptake during seafloor weathering

Andrews (1979) proposed that the partial oxidation of magmatic sulfides at low temperature could account for depletions in S as well as for the observed negative S-isotopic compositions. Because the partial oxidation of sulfide under conditions of limited oxygen supply could lead to the formation of unstable S species of intermediate oxidation state, *i.e.* sulphite SO_3^{2-}, thiosulfate $S_2O_3^{2-}$ and elemental S° (Zhang and Millero, 1993), the following disproportionation reactions may occur:

$$S_2O_3^{2-} + H_2O = H_2S + SO_4^{2-} \quad (7)$$

$$4SO_3^{2-} + 2H^+ = H_2S + 3SO_4^{2-} \quad (8)$$

$$4S° + 4H_2O = 3H_2S + SO_4^{2-} + 2H^+ \quad (9)$$

In principle, equilibrium fractionation of S-isotopes between the oxidized and reduced species in reactions (7), (8) and (9) could lead to enrichment of ^{34}S in sulfate and a corresponding depletion of ^{34}S in sulfide (Ohmoto and Lasaga, 1982). However, the major drawback of this hypothesis is that it requires isotopic exchange between sulfate and sulfonate-sulfur of thiosulfate or sulfide-sulfur before pyrite precipitation. This is highly

309 unlikely, considering the very slow rate, on the order of 10^6 yr, of equilibrium isotopic
310 exchange between sulfide and sulfate at temperature < 100°C (Sakai and Dickson, 1978;
311 Ohmoto and Lasaga, 1982). It has been also shown that the intramolecular isotope
312 exchange of thiosulfate is sufficiently fast to produce isotopically light pyrite even at low
313 temperature, mostly because the sulfonate S of thiosulfate is strongly enriched in ^{34}S
314 relative to the sulfane S (Uyama et al., 1985; Chu et al., 2004). However, the
315 disproportionation of thiosulfate (reaction 7) has been shown to proceed at very slow rates
316 for temperatures below 120°C (Uyama et al., 1985). In addition, recent studies (Bak and
317 Cypionka, 1987; Jorgensen, 1990; Canfield and Thamdrup, 1994; Cypionka et al., 1998;
318 Habicht et al., 1998) have demonstrated that the disproportionation reactions of thiosulfate,
319 sulfite and elemental S in nature are more likely biologically catalyzed processes rather
320 than inorganic reactions at low temperatures (i.e. <100°C).
321
322 Because $\delta^{34}S$ values and S concentration of altered basalts may be controlled by the
323 relative importance of the formation of SO_4^{2-} through complete oxidation (i.e., without
324 isotope fractionation) and, potentially through partial oxidation (i.e., disproportionation) of
325 intermediate S-species, it is possible to predict theoretically the relationship between $\delta^{34}S$
326 values and S concentrations of altered basalts .
327 The distillation equation linking the fraction *F* of S loss during partial sulfide
328 oxidation and the S isotope ratios of the residual S pool ($\delta^{34}S_\beta$) is:
329 $$\delta^{34}S_\beta = (1000+\delta^{34}S_o)*F^{(\alpha-1)} -1000 \quad (10)$$

where $\delta^{34}S_o$ is the initial S isotopic composition of basalt, α the fractionation factor between intermediate S-species and sulfate generated by the reactions of S disproportionation (7), (8) or (9). Examples of relationships between S-isotope composition and S concentration are presented in **Figure 4** for the case of complete S oxidation (i.e. no S-isotope fractionation) and partial oxidation reactions (curves *(d)* and *(c)* of **Fig. 4**, respectively).

We are not aware of experimental investigation of S-isotope fractionation during chemical (i.e. abiotic) disproportionation of intermediate S species which are relevant to low temperature (i.e. <100°C) conditions. Hence, partial S oxidation pathways are calculated using equation (10) in the case of microbial disproportionation reactions where ^{34}S enrichment in sulfate is 13‰. Smaller fractionation factors α near 1.004 can result from microbial disproportionation of thiosulfates (α=1.001) and sulfite (α=1.009) (Habicht et al., 1998) whereas the disproportionation of elemental S will result in larger fractionation factors (α=1.013) (Canfield and Thamdrup, 1994). Smaller fractionation factors or a combination of complete S oxidation and disproportionation will produce S vs. $\delta^{34}S$ relationships lying between model curves (c) and (d) in **Figure 4**. Hence, altered basalts with low S concentrations and $\delta^{34}S$ values are consistent with – but do not necessarily prove – S-isotope fractionation during partial S oxidation reactions. In contrast, altered basalts with negative $\delta^{34}S$ values but higher S concentrations (i.e. lying on the right side of model curve *(c)* in **Fig. 4**) require a net addition of sulfides with low $\delta^{34}S$ values, which likely derived from the bacterial reduction of seawater sulfate.

In order to evaluate the effect of the addition of sulfide derived from the bacterial reduction of seawater sulfate with low $\delta^{34}S$ values, we calculated the theoretical mixing (*mix*) between basaltic S (*bas*) and biogenic S (*bio*) using the relation :

$$\delta^{34}S_{mix} = (S_{bio}\ \delta^{34}S_{bio} + S_{bas}\ \delta^{34}S_{bas}) / S_{mix} \quad (11)$$

where $\delta^{34}S_{bio}$ is calculated using the difference between $\delta^{34}S$ of Jurassic seawater ($\delta^{34}S$ ~15‰, Claypool et al., 1980) and the fractionation factor during bacterial sulfate reduction. As presented in **Figure 4,** all basalt samples (except one sample at 871m depth) require a fractionation factor $\alpha_{SO4\text{-}H2S}$ larger than ~ 1.025 (curve *(a),* **Fig. 4**) in order to produce the observed $\delta^{34}S$ vs. S concentration relationships. The addition of S with highly negative $\delta^{34}S$ values are further confirmed by ion-microprobe analysis of individual pyrite showing the occurrence of $\delta^{34}S$ values down to -45‰.

4.3. Timing of S loss and uptake during low-temperature alteration

Based on the scattered relationship between S concentration and $\delta^{34}S$ values seen in bulk rock (**Fig.4**), it is evident that altered basalts at ODP 801 are affected by a combination of S-depletion during sulfide oxidation and secondary S-enrichment due to bacterial sulfate reduction. In most cases, basalt groundmass is affected by S-loss due to oxidative seafloor weathering whereas saponite or calcite-rich veins may have secondary pyrite enrichment reflecting more reducing conditions. The timing of such S-loss and enrichment is presently unclear but may represent various stages of alteration processes. Alt and Teagle (2003) defined the following multi-stage alteration sequence, which is similar to that described by Talbi and Honnorez (2003). Alteration started in places of high fluid/rock ratio, forming

373 celadonite-rich and Fe-oxyhydroxide alteration halos along fractures. Alteration proceeded
374 away from fractures and into the host rock where lower fluid/rock ratios and more reducing
375 conditions favored the production of smectite and secondary pyrite. As redox conditions
376 changed with time, the formation of phases characteristic of reducing conditions can be
377 observed in previously oxidized rocks. Eventually the entire system became reducing, as
378 demonstrated by the presence of late-stage veins of smectite, calcite, and pyrite. Calcite
379 typically forms the latest minerals that cross-cut all others (Alt and Teagle, 1999) which is
380 consistent with a long duration of alteration (> 50 Ma) as suggested by heat flow data and
381 isotopic ages of secondary phases from the oceanic crust (Staudigel, 2003). Hence,
382 precipitation of secondary pyrite in veins at Site 801 may continue for protracted periods,
383 possibly up to 50 Ma after crust formation of ridge axis. This hypothesis is also consistent
384 with a recent study of Re and Os concentrations and Os isotopic ratios in altered basalt at
385 ODP Site 801 (Reisberg et al., 2007) which suggest significant Re uptake during low-
386 temperature alteration. Model ages of Re addition for altered basalts range from 78 to 160
387 Ma, which likely represent the average ages of long-lived processes rather than specific
388 events. Since secondary pyrite may have accommodated an important part of the input Re
389 (Reisberg et al., 2007), these relatively young model ages suggest that secondary pyrite
390 precipitation may continue for tens of millions of years after crust formation.

391 Microbial communities that colonise the basaltic surface layer at mid-oceanic ridges
392 may become buried below several hundred meters during seafloor spreading and ageing of
393 the oceanic crust. The microbial community may either die during burial or persist to
394 generate deep biosphere in the ocean crust. The highly negative and heterogeneous $\delta^{34}S$

values of late-stage pyrite found at a depth of up to 834 mbsf (*i.e.* 340 m into the basement) demonstrate there is active S-based metabolism during aging of the altered ocean crust at ODP Site 801.

4.4. ^{34}S - ^{33}S - ^{32}S isotope biosignatures in secondary sulfides in oceanic basement

Multiple-sulfur isotope systems provide unique constraints that are not attainable by conventional $\delta^{34}S$ analyses alone (Farquhar et al., 2003; Johnston et al., 2005; Ono et al., 2006). The isotope composition of primordial sulfur (e.g. primary sulfide in basalt) is defined at $\Delta^{33}S = 0‰$ (Fig. 5). Analyses of modern seafloor hydrothermal sulfide minerals and vent fluid H_2S show a slight enrichment of ^{33}S (<0.03 ‰) which is interpreted to reflect local isotope exchange between seawater sulfate and vent sulfide at temperatures >300°C occurring near or at the seafloor (Ono et al., 2007). In contrast, biogenic sulfide data (Ono et al., 2007) plot above the equilibrium mass-dependent fractionation line between SO_4^{2-} and H_2S ($^{33}\alpha \approx {}^{34}\alpha^{0.515}$, Fig. 5), consistent with experimental studies showing that microbial sulfate reduction follows a slightly different mass-dependent law ($^{33}\alpha \approx {}^{34}\alpha^{0.512}$, (Farquhar et al., 2003; Johnston et al., 2005).

Results of multiple-sulfur isotope analyses at ODP Site 801 are presented in **Figure 5** and define a unique domain in $\delta^{34}S$ vs. $\Delta^{33}S$ relationships which is strikingly different from natural hydrothermal and sedimentary biogenic pyrite measured in previous studies (Ono et al., 2006; Ono et al., 2007). These data show at least two generations of secondary pyrite in altered basalt. One is depleted in ^{34}S with $\delta^{34}S$ ranging from –34.5 to –41.5‰, and plots on the equilibrium mass-fractionation line with respect to seawater sulfate, suggesting

417 that these sulfides are derived from reduction of seawater sulfate through near equilibrium
418 processes. The apparent equilibrium isotope fractionation factor α between sulfate and
419 sulfide ranges from 1.056 to 1.062 which corresponds to an equilibration temperature of
420 ~60ºC, consistent with the estimated temperature of basalt alteration (Alt and Teagle,
421 2003). In Figure 5, the equilibrium fractionation line is calculated based on equilibrium S-
422 isotope fractionation between H_2S and present day seawater sulfate (Ono et al., 2007).
423 Since the $\delta^{34}S$ of seawater sulfate has varied in the past, increasing from the present day
424 value of 21‰ to about 23‰ in the Miocene, then decreasing to about 15‰ in the lower
425 Cretaceous (Claypool et al., 1980), $\Delta^{33}S$ values of seawater sulfate would have been also
426 different for the past. Multiple S-isotope analysis of carbonate-associated sulfate of Jurrasic
427 age (184-176 Ma) (Ono and Lyons, unpub results), however, yield $\Delta^{33}S$ values between
428 0.001 to 0.02‰, which are not significantly different from that of modern seawater (**Fig. 5**).
429 Another set of sulfides are characterized by intermediate $\delta^{34}S$ values ranging from –
430 21.4 to –25.8‰ and plot below the equilibrium mass-fractionation line. In order to evaluate
431 the relationships between these two groups of data, we calculated various mixing lines in
432 $\delta^{34}S$ vs. $\Delta^{33}S$ coordinates (**Figure 5**) between secondary pyrite and magmatic sulfides. The
433 results suggest that pyrite with $\delta^{34}S$ values ranging from –21.4 to –25.8‰ are best
434 explained by mixing of primary basaltic sulfide with sulfides that are isotopically
435 equilibrated with seawater sulfate and having $\delta^{34}S$ values < -34.5 ‰. In one case, it appears
436 that the addition of secondary pyrite with $\delta^{34}S$ as low as -50 ‰ is required for sample
437 801C-9R1 but such extremely depleted $\delta^{34}S$ values have not been found using in-situ
438 techniques.

439 The most striking feature of the multiple-sulfur isotope systematics at ODP Site 801
440 is the demonstration of near-equilibrium isotope exchange between pyrite and seawater
441 sulfate at temperature below 100ºC. Extrapolating the rate law obtained for high
442 temperature experiments to 70ºC, the timescale for 90 % isotope exchange between SO_4^{2-}
443 and H_2S, is on the order of 10^7 years (Ohmoto and Lasaga, 1982; Sakai, 1983). Considering
444 that pyrite formed relatively rapidly in altered basalts due to the abundance of reactive Fe
445 for pyrite formation in altered basalt (e.g. Fe-oxyhydroxides along veins and alteration
446 halos), it is likely that the H_2S residence time is shorter than the timescale of isotope
447 exchange between H_2S and SO_4^{2-}. Once pyrite formed, the rate of heterogeneous isotope
448 exchange between seawater SO_4^{2-} and pyrite can be considered negligible and pyrite would
449 preserve its initial $\delta^{34}S$ value. Hence, such large isotope fractionation factors in pyrite
450 reflect more likely biologically catalyzed processes (i.e. enzyme-catalyzed) rather than
451 inorganic reactions.

452 It is important to note that questions remain about the magnitude of isotope
453 fractionation during microbial sulfate reduction. Culture studies have shows a maximum
454 fractionation factor of 45‰ (e.g. Canfield, 2002) although fractionations as low as 2‰ and
455 as large as 72‰ have been also observed in natural samples (Chambers and Trudinger,
456 1979; Detmers et al., 2001; Wortmann et al., 2001). As proposed previously for
457 sedimentary sulfides (Canfield and Thamdrup, 1994), bacterial disproportionation of
458 intermediate S-species is thought to be required to explain sulfide having $\delta^{34}S$ values lower
459 than –45‰ with respect to sulfate (Canfield and Teske, 1996).

460 Culture based studies by Johnston et al. (2005) and Farquhar et al. (2003) have
461 determined $\delta^{34}S$ and $\Delta^{33}S$ relationships for sulfur compounds associated with dissimilatory
462 sulfate reduction, elemental sulfur disproportionation and sulfite disproportionation. These
463 studies showed that sulfide produced by sulfate reduction follows a trajectory along the
464 biological sulfate reduction line ($^{33}\alpha \approx {}^{34}\alpha^{0.512}$) as presented in **Figure 5**. These studies also
465 showed that sulfite disproportionation follows a similar relationship ($^{33}\alpha \approx {}^{34}\alpha^{0.512}$) when
466 isotope ratios of sulfide are compared with those of reactant (e.g. sulfite). According to
467 Table 2 of Johnston et al. (2005), the mass-dependent exponent $^{33}\theta$ values during sulfite
468 disproportionation range from 0.5103 to 0.5107 for *D. thiozymogenes* and 0.512 for *D.*
469 *sulfodismutans* when $^{33}\theta$ values are calculated between substrate and product pairs (i.e.,
470 sulfite and sulfide) and not between two products (i.e., sulfate and sulfide). These $^{33}\theta$
471 values are within the range for sulfate reducers ($^{33}\theta$ between 0.5077 to 0.5125) considering
472 sulfate-sulfide pairs (Farquhar et al., 2003; Johnston et al., 2005; Johnston et al., 2007).
473 Thus, additional isotope effect associated with disproportionation of intermediate sulfur
474 species would still follow the biological fractionation line defined by sulfate reducers.
475 Using available experimental studies, it is therefore difficult to explain our data from 801C
476 that show equilibrium with seawater sulfate using available experimental studies. Different
477 environmental factors and growth conditions may result in different multiple-sulfur isotope
478 relationships between natural systems and culture experiments. In particular, pure culture
479 experiments, such as those performed by Johnston et al. (2005) are optimized for a
480 maximum growth with organic substrate in excess. In contrast, natural sulfate reducing
481 bacteria populations may frequently experience organic substrate-limitation in the

environment and generally represent a higher diversity of populations which are not investigated in pure culture fractionation studies.

Considering the putative very low metabolic activity of the deep bacterial biosphere (Parkes et al., 1994; D'Hondt et al., 2002), it is likely that bacterial sulfur metabolisms in altered basement proceeds at a very low rate. Hence, we tentatively interpret the equilibrium S-isotope fractionation between seawater sulfate and secondary pyrite at 801 as the result of bacterial sulfate reduction proceeding at very slow rate with significant back-oxidation of sulfide due to bacterial disproportionation or abiotic reactions. Such a feature may be expected for S metabolism that is limited by nutrient and energy availabilities, consistent with endolithic communities in altered oceanic crust.

4.5 S-isotope budget and implication for the significance of the deep biosphere in volcanic basement

Based on the analysis of the SUPER composite, the bulk altered tholeiitic section recovered in Hole 801C yields an average S concentration of 0.09%, which corresponds to a net loss of ca. 30-40% of basaltic S during seafloor weathering (considering that S concentration of the fresh crystalline 801C basalt section is between 0.17 and 0.12 wt%). This confirms previous studies showing that the upper 300m of the oceanic crust have undergone a net depletion in S due to primary sulfide oxidation (Andrews, 1979; Alt, 1995). However, S-isotope composition of the SUPER composite yields negative $\delta^{34}S$ values of –6.8‰, suggesting significant S gain due to bacterial sulfate reduction that only partially offsets the S loss during seafloor weathering.

504 Using mass balance considerations between end-member biogenic S with minimum
505 $\delta^{34}S$ values at around -40‰ and igneous sulfides ($\delta^{34}S$ = 0‰), we calculate that, on
506 average, a minimum of ca. 17% of pyrite-S in altered basalts at Site 801 is derived from
507 bacterial reduction of seawater sulfate. This translates into a minimum of ca. 5 μmol/g of
508 seawater sulfate that is reduced and added to the crust. Using an upper crustal section of
509 440 m of 165 Ma-old altered crust with an average density of 2.8 g/cm^3, we calculate a
510 minimum global flux of bacterially reduced sulfate in the upper basaltic crust of ca. $4x10^{-9}$
511 mol cm^{-2} year^{-1}. Recent estimates of subsurface microbial activity in marine sediments
512 suggest a global sulfate flux of $2.8x10^{-9}$ to $13x10^{-9}$ mol cm^{-2} year^{-1} for sulfate-rich open-
513 ocean sites (D'Hondt et al., 2002). Hence, our results suggest that bacterial sulfate reduction
514 within the basaltic crust may be comparable to that in deep-seated heterotrophic systems
515 but is still at least two to three orders of magnitude lower than at ocean-margin sites.

516 An important aspect of this study is the question of the energy source available to
517 sustain microbial metabolism in basaltic basement. Previous studies suggested that
518 autotrophic organisms such as Fe-oxidizers may be present in the youngest basalts formed
519 at Mid Oceanic Ridges, whereas older basalts seem to be dominated by heterotrophic
520 organisms (Thorseth et al., 2001). In addition to the potential C-sources available from
521 primary biomass production, supplemental sources of organic C may exist when advective
522 or diffusive exchange takes place between sediment pore waters and basalt aquifers.
523 Although the sediments at Site 801 are mostly oxidized pelagic sediments, with low organic
524 carbon content (Alt and Burdett, 1992), it is possible that a significant source of nutrient
525 and electron donors such as CH_4 and NH_4^+ may be transported from the overlying sediment

across the sediment/basement interface (D'Hondt et al., 2004) without significant H_2S production in the sediments. Production of small quantities of H_2 during seawater/basalt interactions may also support significant autotrophic sulfate reducer communities (Bach and Edwards, 2003) such as those suggested to be active during seafloor serpentinization at low temperatures (Alt and Shanks, 1998). Although the nature of electron donors (H_2 or organic matter) in basaltic ridge flank systems is uncertain, our results show they provide an important fuel for microbial sulfate reduction.

We note that that no additional source of energy is needed to sustain a population of S-disproportionating bacteria because only CO_2 serves as a carbon source (Bak and Cypionka, 1987; Cypionka et al., 1998). Bacteria able to disproportionate chemolithotrophically inorganic compounds appear to be widespread in anoxic sediments (Thamdrup et al., 1993) and they could be also present in basaltic environments. Because several strains of sulfate reducing bacteria can also develop S disproportionation-based metabolism (Cypionka et al., 1998), microbial communities in the basaltic crust could potentially adapt to changing C-sources and sulfate availability.

5. CONCLUSIONS

Previous studies have reported ubiquitous fractionation of sulfur isotopes in altered volcanic rocks but interpretations based on abiotic fractionation between intermediate sulfur species formed during basalt alteration have been preferred. In this paper, we revisited the use of S isotopes as biosignatures in altered oceanic crust at ODP Site 801. I*n*-

549 *situ* ion probe $\delta^{34}S$ analyses were used to enable fine scale assessment of isotopic variations
550 in secondary sulfides and revealed highly negative ($\delta^{34}S$ down to -45‰) and heterogeneous
551 $\delta^{34}S$ values found at a depth of 834 m below seafloor (*i.e.* 340 m into the basement). These
552 results constitute among the clearest evidence for widespread microbial activity in basaltic
553 ocean crust. Bulk rock S concentrations ranging from 0.02% up to 1.28% and $\delta^{34}S$ values
554 ranging from 0.9‰ to -16‰ are consistent with loss of magmatic primary mono-sulfide
555 and addition of secondary sulfide via microbial sulfate reduction. High-precision multiple
556 S-isotope (^{32}S,^{33}S,^{34}S) analyses show that secondary sulfides exhibit mass-dependant
557 equilibrium fractionation relative to seawater sulfate, consistent with sulfate reduction at
558 low temperature, below 70°C. The relationship between $\Delta^{33}S$ and $\delta^{34}S$ values suggests that
559 bacterial sulfate reduction proceeds at very low metabolic rates. Finally, the determination
560 of the S-isotope composition of bulk altered oceanic crust demonstrates that S-based
561 metabolic activity of subsurface life in oceanic basalt is widespread, and can affect the
562 global S budget in oceanic crust.

563 Although it is possible that secondary pyrite at Site 801 may form during protracted
564 periods, probably up to 50 Ma after crust formation of ridge axis, additional work is
565 required to better constraints the timing of microbial activity. Microbial communities that
566 colonize the basaltic surface layer at mid-oceanic ridges may become buried below several
567 hundred meters during seafloor spreading and aging of the oceanic crust, but could also
568 enter the basement during fluid exchange with overlying sediments as the crust is buried.
569 Identifying and culturing these widespread deep-endolithic microorganisms in igneous
570 oceanic basement may provide a unique opportunity to test the metabolic limit of microbial

571 life, its relationship with the subsurface biosphere in sediments and its role in affecting
572 chemical exchange between the ocean and lithosphere.
573

ACKNOWLEDGMENT

The technical help of Michel Champenois on ion microprobe is gratefully acknowledged. We thank Luc Marin for S concentration analyses. Ion-probe and chemical analysis have been supported by INSU-CNRS. Alt's contribution was supported by NSF OCE-0424558 and OCE-0622949. Rouxel's contribution was supported by NSF OCE-0622982 and Frank and Lisina Hoch Endowed Fund. Ono thanks Agouron Institute and NSF OCE-0753126 for funding. This research used samples and/or data provided by the Ocean Drilling Program. The ODP is sponsored by the US National Science Foundation (NSF) and participating countries under the management of Joint Oceanographic Institutions (JOI). The work benefited from fruitful discussions and comments by W. Bach, K. Edwards, J. Hayes and T. Lyons, B. Wing and two anonymous reviewers.

REFERENCES CITED

Alt, J.C., 1995. Sulfur isotopic profile through the oceanic crust: Sulfur mobility and seawater-crustal sulfur exchange during hydrothermal alteration. Geology, 23: 585-588.

Alt, J.C. and Burdett, J.W., 1992. Sulfur in pacific deep-sea sediments (leg 129) and implications for cycling of sediment in subduction zones. In: R.L. Larson and Y. Lancelot (Editors), Proc. ODP, Sci. Res. 129. Ocean Drilling Program, College Station, TX, pp. 283-294.

Alt, J.C., Davidson, G.J., Teagle, D.A.H. and Karson, J.A., 2003. Isotopic composition of gypsum in the Macquarie Island ophiolite: Implications for the sulfur cycle and the subsurface biosphere in oceanic crust. Geology. 31, 549-552.

Alt, J.C. and Shanks, W.C., 1998. Sulfur in serpentinized oceanic peridotites: Serpentinization processes and microbial sulfate reduction. J. Geophys. Res., 103, 9917-9929.

Alt, J.C. and Teagle, D.A.H., 1999. The uptake of carbon during alteration of ocean crust. Geochim. Cosmochim. Acta, 63, 1527-1535.

Alt, J.C. and Teagle, D.A.H., 2003. Hydrothermal alteration of upper oceanic crust formed at a fast-spreading ridge: mineral, chemical, and isotopic evidence from ODP Site 801. Chem. Geol., 201, 191-211.

Andrews, A.J., 1979. On the effect of low-temperature seawater interaction on the distribution of sulfur in oceanic crust, layer 2. Earth Planet. Sci. Lett., 46, 68-80.

Bach, W. and Edwards, K.J., 2003. Iron and sulfide oxidation within the basaltic ocean crust: Implications for chemolithoautotrophic microbial biomass production. Geochim. Cosmochim. Acta, 67, 3871-3887.

Bak, F. and Cypionka, H., 1987. A novel type of energy metabolism involving fermentation of inorganic compounds. Nature, 326, 891-892.

Canfield, D.E., 2002. Biogeochemistry of sulfur isotopes. In: J.W. Valley and D.R. Cole (Editors), Stable isotope geochemistry: Mineralogical Society of America. Reviews in Mineralogy, pp. 607-633.

Canfield, D.E., Raiswell, R., Westrich, J.T., Reaves, C.M. and Berner, R.A., 1986. The use of chromium reduction in the analysis of reduced inorganic sulfur in sediments and shales. Chem. Geol. 54, 149-155.

Canfield, D.E. and Teske, A., 1996. Late Proterozoic rise in atmospheric oxygen concentration inferred from phylogenetic and sulphur-isotope studies. Nature. 382, 127-132.

Canfield, D.E. and Thamdrup, B., 1994. The production of 34S depleted sulfide during bacteial disproportionation of elemental sulfur. Science, 266, 1973-1975.

Chambers, L.A. and Trudinger, P.A., 1979. Microbiological fractionation of stable sulfur isotopes: a review and critique. Geomicrobiol. J., 1, 249-293.

Chaussidon, M. and Demange, J.C., 1988. Instrumental mass fractionation in ion microprobe studies of sulphur isotopic ratios. In: A. Benninghoven, A.M. Huber and H.W. Werner (Editors), Secondary Ion Mass Spectrometry VI. John Wiley Sons, New York, pp. 937-940.

630 Chu, X., Ohmoto, H. and Cole, D.R., 2004. Kinetics of sulfur isotope exchange between
631 aqueous sulfide and thiosulfate involving intra- and intermolecular reactions at
632 hydrothermal conditions. Chem. Geol., 211, 217-235.
633 Claypool, G.C., Holser, W.T., Kaplan, I.R., Sakai, H. and Zak, I., 1980. The age curves of
634 sulfur and oxygen isotopes in marine sulfate and their mutual interpretations. Chem.
635 Geol., 28, 199-260.
636 Coplen, T.B. and Krouse, H.R., 1998. Sulphur isotope data consistency improved. Nature,
637 392, 32.
638 Cypionka, H., Smock, A. and Böttcher, M.E., 1998. A combined pathway of sulfur
639 compound disproportionation in Desulfovibrio desulfuricans. FEMS Microbiol.
640 Lett, 166, 181-186.
641 D'Hondt, S., Jorgensen, B.B., Miller, D.J. and etal, 2004. Distributions of Microbial
642 Activities in Deep Subseafloor Sediments. Science, 306, 2216-2221.
643 D'Hondt, S., Rutherford, S. and Spivack, A., 2002. Metabolic Activity of Subsurface Life in
644 Deep-Sea Sediments. Science, 295, 2067-2070.
645 Detmers, J., Bruchert, V., Habicht, K.S. and Kuever, J., 2001. Diversity of sulfur isotope
646 fractionation by sulfate-reducing prokaryotes. Appl. Environ. Microbiol., 67, 888-
647 894.
648 Farquhar, J. et al., 2003. Multiple sulphur isotopic interpretations of biosynthetic pathways;
649 implications for biological signatures in the sulphur isotope record. Geobiology, 1,
650 27-36.
651 Field, C.W., Dymond, J.R., Heath, G.R., Corliss, J.B. and Dasch, E.J., 1976. Sulfur isotope
652 reconnaissance of epigenetic pyrite in ocean-floor basalts, Leg 34 and elsewhere,
653 Initial Reports of the DSDP, vol. 34, pp. 381-384.
654 Fisk, M. and Kelley, K., 2002. Probing the Pacific's oldest MORB glass: mantle chemistry
655 and melting conditions during the birth of the Pacific Plate. Earth Planet. Sci. Lett.,
656 202, 741-752.
657 Fisk, M.R., Giovannoni, S.J. and Thorseth, I.H., 1998. Alteration of oceanic volcanic glass:
658 textural evidence of microbial activity. Science, 281, 978-980.
659 Furnes, H., Muehlenbachs, K., Torsvik, T., Thorseth, I.H. and Tumyr, O., 2001. Microbial
660 fractionation of carbon isotopes in altered basaltic glass from the Atlantic Ocean,
661 Lau Basin and Costa Rica Rift. Chemical Geology, 173, 313-330.
662 Gao, X. and Thiemens, M.H., 1991. Systematic study of sulfur isotopic composition in iron
663 meteorites and the occurrence of excess 33S and 36S. Geochim. Cosmochim. Acta,
664 55, 2671-2679.
665 Govindaraju, K. and Mevelle, G., 1987. Fully automated dissolution and separation
666 methods for inductively coupled plasma-atomic emission spectrometry rock
667 analysis. Apllication to the determination of rare earth elements. J. Anal. Atom.
668 Spectro., 2, 615-621.
669 Habicht, K.S., Canfield, D.E. and Rethmeier, J., 1998. Sulfur isotope fractionation during
670 bacterial reduction and disproportionation of thiosulfate and sulfite. Geochim.
671 Cosmochim. Acta, 62, 2585-2595.
672 Hu, G.X., Rumble, D. and Wang, P.L., 2003. An ultraviolet laser microprobe for the insitu
673 analysis of multisulfur isotopes and its use in measuring Archean sulfur isotope
674 mass-independent anomalies. Geochim. Cosmochim. Acta, 67, 3101-3118.

675 Hulston, J.R. and Thode, H.G., 1965. Variations in the S33, S34, and S36 contents of
676 meteorites and their relation to chemical and nuclear effects. J. Geophys. Res., 70,
677 3475-3484.
678 Johnston, D.T., Farquhar, J. and Canfield, D.E., 2007. Sulfur isotope insights into microbial
679 sulfate reduction: When microbes meet models. Geochim. Cosmochim. Acta, 71,
680 3929-3947.
681 Johnston, D.T. et al., 2005. Multiple sulfur isotope fractionations in biological systems: a
682 case study with sulfate reducers and sulfur disproportionators. Am. J. Sci., 305, 645-
683 660.
684 Jorgensen, B.B., 1990. A thiosulfate shunt in the sulfur cycle of marine sediments. Science,
685 249, 152-154.
686 Kelley, K.A., Plank, T., Ludden, J. and Staudigel, H., 2003. Composition of altered oceanic
687 crust at ODP Sites 801 and 1149. Geochem. Geophys. Geosys., 4,
688 doi:10.1029/2002GC000435.
689 Koppers, A.A.P., Staudigel, H. and Duncan, R.A., 2003. High-resolution 40Ar/39Ar dating
690 of the oldest oceanic basement basalts in the western Pacific basin. Geochem.
691 Geophys. Geosyst., 4, doi: 10.1029/2003GC000574.
692 Krouse, H.R., Brown, H.M. and Farquharson, R.B., 1977. Sulphur isotope compositions of
693 sulphides and sulphates, DSDP Leg 37. Can. J. Earth Sci., 14, 787-793.
694 Larson, R.L., Lancelot, Y. and ShipboardScientificParty, 1992. Proc. ODP, Sci. Results,
695 129, CollegeStation, TX.
696 Miller, M.F., 2002. Isotopic fractionation and the quantification of 17O anomalies in the
697 oxygen three-isotope system; an appraisal and geochemical significance. Geochim.
698 Cosmochim. Acta, 66, 1881-1889.
699 Moore, J.G. and Fabbi, B.P., 1971. An estimate of the juvenile sulfur content of basalt.
700 Contrib. Mineral. Petrol., 41, 105-118.
701 Ohmoto, H. and Lasaga, A.C., 1982. Kinetics of reactions between aqueous sulfates and
702 sulfides in hydrothermal systems. Geochim. Cosmochim. Acta, 46, 1727-1745.
703 Ono, S., ShanksIII, W.C., Rouxel, O.J. and Rumble, D., 2007. Multiple-sulfur isotope
704 constraints on the seawater sulfate contribution in modern seafloor hydrothermal
705 sulfide. Geochem. Cosmochim. Acta, 71, 1170-1182.
706 Ono, S., Wing, B.A., Johnston, D., Farquhar, J. and Rumble, D., 2006. Mass-dependent
707 fractionation of quadruple sulfur isotope system as a new tracer of sulfur
708 biogeochemical cycles. Geochim. Cosmochim. Acta, 70, 2238-2252.
709 Parkes, R.J. et al., 1994. Deep bacterial biosphere in Pacific Ocean sediments. Nature, 371,
710 410-413.
711 Plank, T., Ludden, J.N., Escutia, C. and am, e., 2000. Proc. ODP, Init Repts., 185, College
712 Station (TX).
713 Pockalny, R.A. and Larson, R.L., 2003. Implications for crustal accretion at fast spreading
714 ridges from observations in Jurassic oceanic crust in the western Pacific. Geochem.
715 Geophys. Geosyst., 4, doi:10.1029/2001GC000274.
716 Pringle, M., 1992. Radiometric ages of basaltic basement recovered at Sites 800, 801, and
717 802, Leg 129, western Pacific Ocean. In: Y.L. R.L. Larson, A. Fisher and E.L.
718 Winterer (Editor), Proc. Ocean Drill. Program, Sci. Results, 129. Ocean Drilling
719 Program, Texas A&M University, College Station,, pp. 389-404.

720 Puchelt, H., Prichard, H.M., Berner, Z. and Maynard, J., 1996. Sulfide mineralogy, sulfur
721 content, and sulfur isotope composition of mafic and ultramafic rocks from Leg
722 147. Proceedings of the Ocean Drilling Program, Scientific Results : College
723 Station, TX (Ocean Drilling Program), 147, 91-101.
724 Reisberg, L., Rouxel, O., Ludden, J., Staudigel, H. and Zimmermann, C., 2007. Re-Os
725 results from ODP Site 801: Evidence for extensive Re uptake during alteration of
726 oceanic crust. Chem. Geol. (in press).
727 Revillon, S., Barr, S.R., Brewer, T.S., Harvey, P.K. and Tarney, J., 2002. An alternative
728 approach using integrated gamma-ray and geochemical data to estimate the inputs to
729 subduction zones from ODP Leg 185, Site 801. Geochem. Geophys. Geosys., 3,
730 doi: 10.1029/2002GC000344.
731 Rice, C.A., Tuttle, M.L. and Reynolds, R.L., 1993. The analysis of forms of sulfur in
732 ancient sediments and sedimentary rocks: comments and cautions:. Chemical
733 Geology, 107, 83-95.
734 Sakai, H., 1983. Sulfur isotope exchange rate between sulfate and sulfide and its
735 application. Geothermics, 12, 111-117.
736 Sakai, H. and Dickson, F.W., 1978. Experimental determination of the rate and equilibrium
737 fractionation factors of sulfur isotope exchange between sulfate and sulfide in
738 slightly acid solutions at 300°C and 1000 bars. Earth Planet. Sci. Lett., 30, 151-161.
739 Staudigel, H., 2003. Hydrothermal Alteration Processes. In: H. Holland and K. Turekian
740 (Editors), Treatise of Geochemistry, pp. 511-537.
741 Staudigel, H. and Hart, S.R., 1983. Alteration of basaltic glasses: Mechanisms and
742 significance for the oceanic crust-seawater budget. Geochim. Cosmochim. Acta, 47,
743 337-350.
744 Talbi, E.H. and Honnorez, J., 2003. Low-temperature alteration of Mesozoic oceanic crust,
745 ODP Leg 185. Geochem. Geophys. Geosys., 4, doi:10.1029/2002GC000405.
746 Thamdrup, B., Finster, K., Hansen, W. and Bak, F., 1993. Bacterial disproportionation of
747 elemental sulfur coupled to chemical reduction of iron and manganese. Appl.
748 Environ. Microbiol, 59, 101-108.
749 Thorseth, I.H., Furnes, H. and Heldal, M., 1992. The importance of microbiological activity
750 in the alteration of natural basaltic glass. Geochim. Cosmochim. Acta, 56, 845-850.
751 Thorseth, I.H., Torsvik, T., Torsvik, V., Daae, F.L. and Pedersen, R.B., 2001. Diversity of
752 life in ocean floor basalt. Earth Planet. Sci. Lett., 194, 31-37.
753 Uyama, F., Chiba, H., Kusakabe, M. and Sakai, H., 1985. Sulfur isotope exchange reactions
754 in the aqueous system: Thiosulfate-sulfide-sulfate at hydrothermal temperature.
755 Geochem. J., 19, 301-315.
756 Wortmann, U.G., Bernasconi, S.M. and Bottcher, M.E., 2001. Hypersulfidic deep biosphere
757 indicates extreme sulfur isotope fractionation during single-step microbial sulfate
758 reduction. Geology, 29, 647-650.
759 Young, E.D., Galy, A. and Nagahara, H., 2002. Kinetic and equilibrium mass-dependent
760 isotope fractionation laws in nature and their geochemical and cosmochemical
761 significance. Geochim. Cosmochim. Acta, 66, 1095-1104.
762 Zhang, J.-Z. and Millero, F.J., 1993. The products from the oxidation of H2S in seawater.
763 Geochim. Cosmochim. Acta, 57, 1705-1718.
764

765

766 **Figure Captions**

767

768 **Figure 1.** Map of the West Pacific (Izu and Mariana arcs) and location of ODP Hole 801C
769 drilled during Leg 129 and 185. Modified after Plank et al. (2000).

770

771 **Figure 2.** Downhole $\delta^{34}S$ composition of sulfides in Hole 801C. Simplified stratigraphic
772 column of basaltic basement is shown with the depth scale. S-isotope compositions
773 obtained by ion-microprobe for individual pyrite and marcasite minerals are marked by
774 crosses while pyrite separates analyzed for multiple S-isotopes and conventional gas-source
775 mass spectrometers are marked by gray and black circles respectively. Gray and black
776 diamonds correspond to bulk rock S isotope analysis for AVS and Cr-S respectively.
777 Dashed vertical line represents the S isotope composition of fresh basalts. H.D = Si-Fe-rich
778 hydrothermal deposit. ALK = Alkaline basalts. MORB = mid-ocean ridge basalts. Error
779 bars for ion microprobe is 2 per mil whereas the error bars on the gray and black symbols
780 are 0.2 per mil.

781

782 **Figure 3.** photomicrograph of pyrite and marcasite analysed by ion microprobe with
783 corresponding $\delta^{34}S$ values. (a) 801C-43R1,29/v; large polycrystalline aggregate of
784 marcasite in 2cm thick carbonate vein; (b) 801C-6R5,75; pyrite lining carbonate-rich vein;
785 (c) sample 801C-9R1,32; marcasite enrichment in alteration halo; (d) 801C-17R1,100;
786 pyrite in thin vein associated with saponite; (e) 801C-23R1,45; pyrite enrichment in basalt

787 associated with vesicles filled with carbonate; (f) 801C-27R1,50; pyrite-rich patch within
788 microdolerite with titanomagnetite needles intergrowth.
789
790 **Figure 4.** Plot of S concentration versus S isotope composition of whole altered basalts at
791 Site 801 (diamonds). The SUPER composite, representative of the bulk altered crust at Site
792 801 and fresh basalt are plotted for comparison. Arrows represent schematic trends. Curves
793 *(a)* and *(b)* represent mixing lines between fresh basalt and secondary sulfides formed
794 through dissimilatory sulfate reduction with fractionation factors of 1.025 and 1.045
795 respectively. Curve *(c)* represents possible evolutions of S concentration and $\delta^{34}S$ values
796 during partial oxidation of igneous sulfides proceeding through disproportionation reactions
797 and following a Rayleigh-type fractionation process (fractionation factor between forming
798 SO_4^{2-} and intermediate S-species is taken at 1.013 after Canfield and Thamdrup (1994)).
799 Curve *(d)* represents the trend for primary sulfide dissolution (i.e. quantitative leaching).
800
801 **Figure 5.** $\delta^{34}S$ vs. $\Delta^{33}S$ and $\delta^{34}S^*$ vs. $\Delta^{33}S^*$ compositions of secondary sulfides from Site
802 801 compared with sedimentary biogenic sulfides (Ono et al., 2006) and hydrothermal
803 pyrite from mid-ocean ridges (Ono et al., 2007). MORB=Mid-Ocean Ridge Basalt,
804 estimated from the analysis of Canyon Diablo Troilite (CDT) which is representative of
805 primordial sulfur in fresh mid-ocean ridge basalt (Ono et al., 2007). SW = modern to
806 Jurassic seawater determined by the analysis of carbonate-associated sulfate (Ono and
807 Lyons, unpub results) and modern marine sulfate (Ono et al., 2007). Various examples of
808 mixing lines between igneous S and secondary sulfides from Site 801 are plotted. The

809 isotope composition of H_2S in isotope equilibrium with seawater SO_4^{2-} (SW) as a function
810 of temperature is described by the solid black line (after Ono et al., 2007). The isotope
811 composition of H_2S produced by bacterial sulfate reduction using fractionation lines
812 experimentally determined by Farquhar et al. (2003) is also shown for comparison.

813
814
815
816

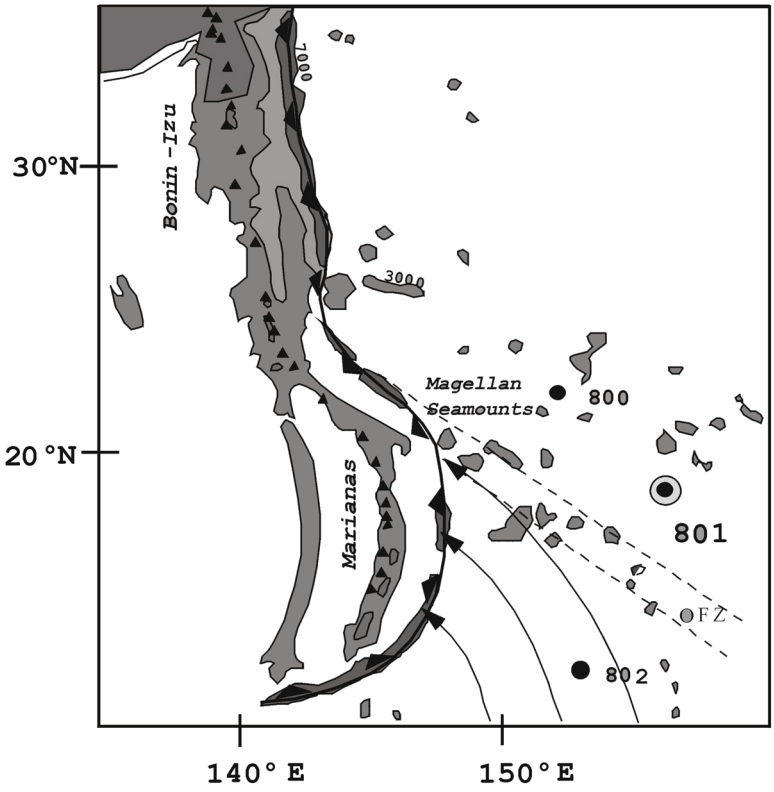
30°N
20 °N
140° E
150° E
Bonin -Izu
Marianas
Magellan
Seamounts
800
801
802
FZ
2000
3000

Figure 1

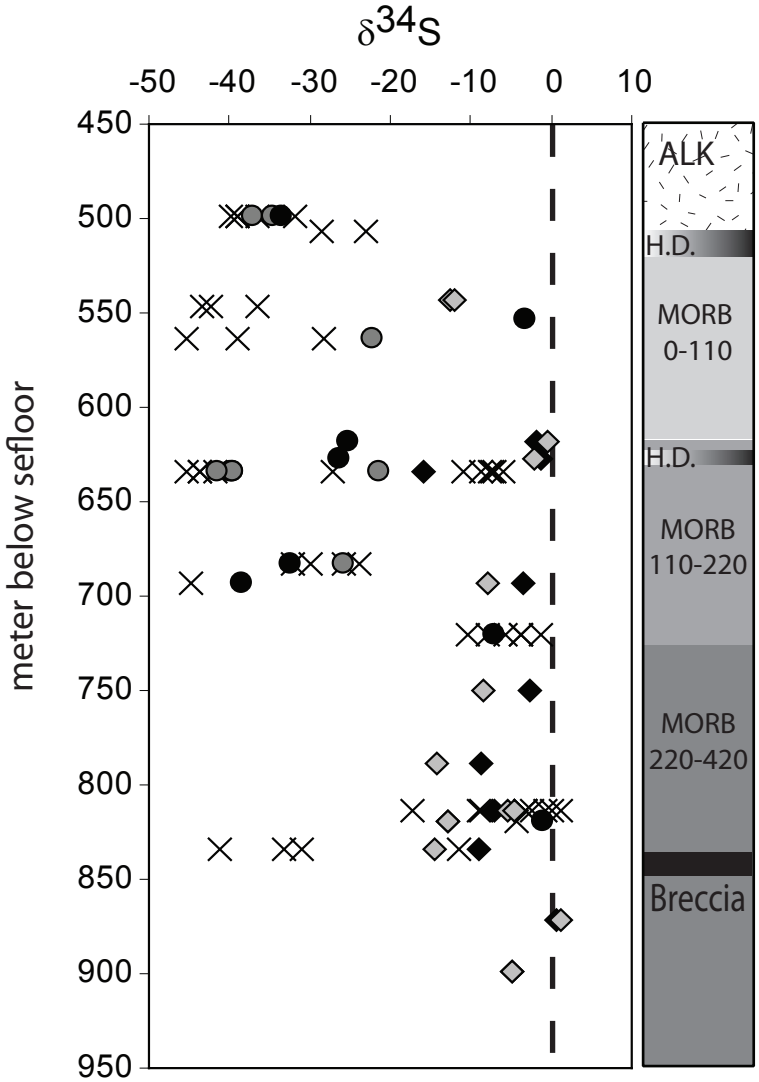
δ34S
-50
-40
-30
-20
-10
0
10
meter below sefloor
450
500
550
600
650
700
750
800
850
900
950
ALK
H.D.
MORB
0-110
H.D.
MORB
110-220
MORB
220-420
Breccia

Figure 2

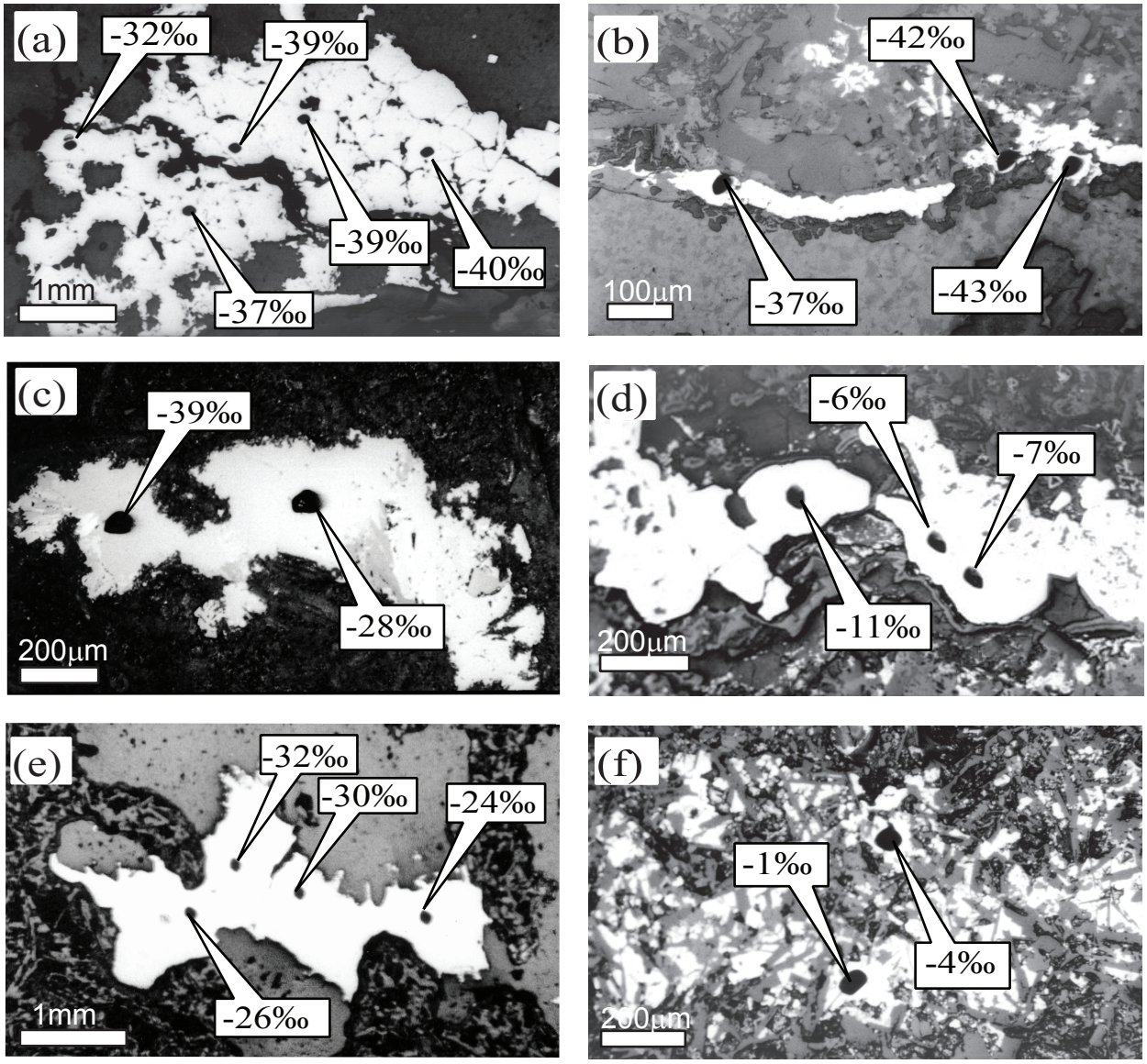
(a)
-32‰
-39‰
-39‰
-40‰
-37‰
1mm
(b)
-42‰
-37‰
-43‰
100μm
(c)
-39‰
-28‰
200μm
(d)
-6‰
-7‰
-11‰
200μm
(e)
-32‰
-30‰
-24‰
-26‰
1mm
(f)
-1‰
-4‰
200μm

Figure 3

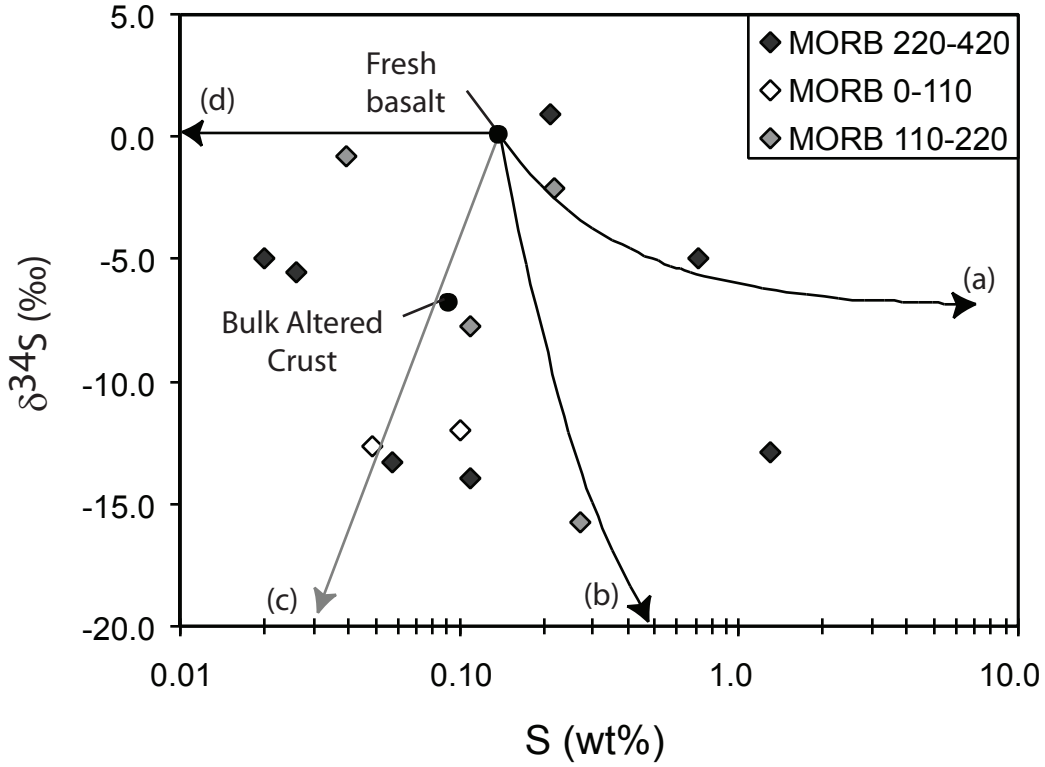
MORB 220-420
MORB 0-110
MORB 110-220
Fresh basalt
(d)
(a)
(b)
(c)
Bulk Altered Crust
5.0
0.0
-5.0
-10.0
-15.0
-20.0
0.01
0.10
1.0
10.0
δ34S (‰)
S (wt%)

Figure 4

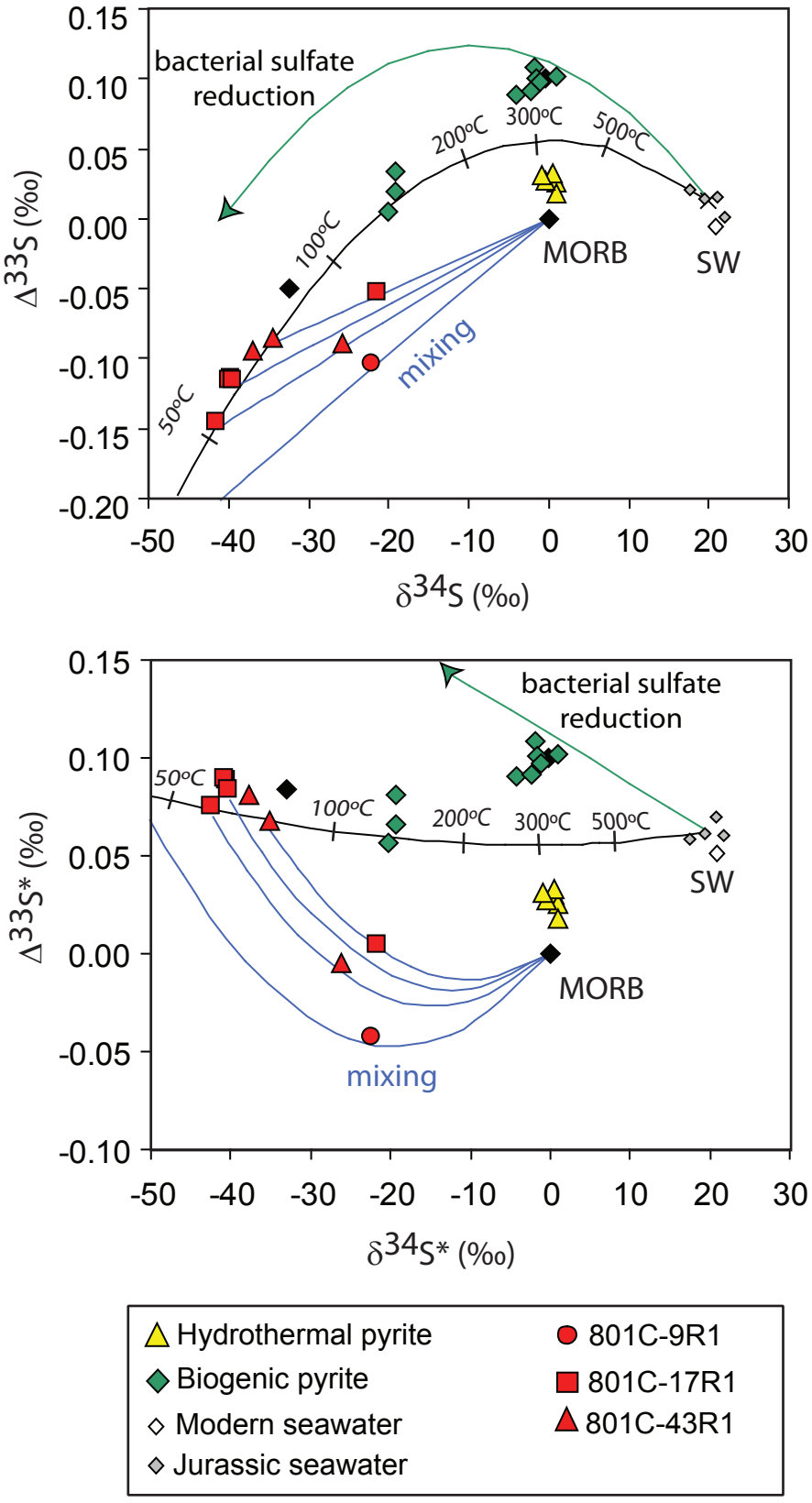
0.15
0.10
0.05
0.00
-0.05
-0.10
-0.15
-0.20
bacterial sulfate reduction
200ºC
300ºC
500ºC
100ºC
MORB
SW
mixing
50ºC
-50 -40 -30 -20 -10 0 10 20 30
Δ33S (‰)
δ34S (‰)
0.15
0.10
0.05
0.00
-0.05
-0.10
bacterial sulfate reduction
50ºC
100ºC
200ºC
300ºC
500ºC
SW
MORB
mixing
-50 -40 -30 -20 -10 0 10 20 30
Δ33S* (‰)
δ34S* (‰)
Hydrothermal pyrite
Biogenic pyrite
Modern seawater
Jurassic seawater
801C-9R1
801C-17R1
801C-43R1

Figure 5

Table 1: Major element chemistry, S concentration and S-isotope composition of altered basalts at Site 801

Sample	Depth	LOI	Al_2O_3	CaO	Fe_2O_3 T	K_2O	MgO	MnO	Na_2O	P_2O_5	SiO_2	TiO_2	ΣS	$\delta^{34}S$	CrS/ΣS*	$\delta^{34}S$	$\delta^{34}S$	$\delta^{34}S$	Description
		(wt%)											(wt%)	ΣS	(%)	AVS	CrS	SO4	
801C-06R3,18	543	6.4	22.1	8.0	3.6	2.6	1.7	<0.05	2.72	0.07	51.6	1.19	0.100	-12.0	97.3		-12.0	-5.6	Highly altered aphyric basalt
801C-06R3,42	544	9.9	21.9	14.1	6.0	0.8	2.4	0.15	3.04	0.07	50.0	1.14	0.049	-12.7	79.5		-12.7	-6.0	Medium altered basalt with carbonate veins
801C-15R4,69	618	4.7	14.8	11.0	12.6	0.1	5.7	0.16	2.79	0.20	46.1	1.85	0.039	-0.8	74.0	-1.9	-0.4		Medium altered basalt with thin saponite veins
801C-15R7,1	621	7.1	19.5	8.2	5.5	0.9	1.5	0.03	3.65	0.20	51.0	2.44	0.051						Highly altered (bleached) basalt
801C-15R7,31	622	9.9	18.4	12.9	5.1	0.5	1.8	0.13	3.44	0.24	46.1	2.17	0.082						Highly altered (bleached) basalt
801C-16R3,82	627	8.3	16.6	6.2	12.1	0.5	2.5	0.10	3.19	0.38	45.3	3.78	0.220	-2.1	94.9	-1.4	-2.2	-2.5	Highly altered basalt
801C-17R1,100	634	3.1	12.7	11.3	15.9	0.1	5.5	0.26	2.53	0.28	46.1	2.71	0.270	-15.8	18.0	-15.8		-2.9	Least altered basalt with pyrite and carbonate-filled vesicules
801C-24R2,36	693	1.7	13.7	11.3	14.7	0.1	6.6	0.26	2.60	0.24	47.2	2.14	0.110	-7.7	95.7	-3.4	-7.9	-7.9	Least altered aphyric basalt
801C-25R1,10	701	1.7	13.7	11.7	14.1	0.0	6.9	0.25	2.68	0.2	48.6	2.0	0.016						Least altered aphyric basalt
801C-34R3,81	789	3.4	12.9	9.4	16.2	0.7	5.3	0.18	2.59	0.22	46.7	2.33	0.057	-13.3	85.6	-8.8	-14.1	-5.2	Medium altered basalt with alteration halos
801C-37R1,83	814	3.5	13.3	10.5	13.7	0.1	6.0	0.22	2.65	0.25	47.5	2.34	0.720	-4.9	84.2	-7.2	-4.5	-3.9	Least altered basalt with carbonate and saponite-filled vesicules
801C-37R1,83/V	814	10.8	6.2	2.0	46.8	0.5	4.8	0.07	0.47	0.11	27.5	1.02	0.026	-5.5			-5.5	1.2	Large celadonite and Fe-oxide vein with carbonate
801C-37R5,30	819	1.6	13.1	10.0	13.5	0.2	5.0	0.22	2.83	0.19	50.9	2.37	1.300	-12.9	47.4	-12.9	-12.9	-8.0	Least altered basalt
801C-39R2,28	834	1.9	13.8	10.8	14.2	0.1	6.9	0.27	2.62	0.23	46.8	2.34	0.110	-14.0	90.2	-9.0	-14.5	-1.9	Least altered aphyric basalt
801C-43R1,13	869	2.2	13.5	11.0	13.3	0.1	6.4	0.23	2.78	0.18	48.5	2.00	0.410						Least altered basalt
801C-43R2,75	871	0.3	14.6	10.7	12.7	0.2	6.5	0.22	3.02	0.26	48.6	2.10	0.210	0.9	29.5	0.8	1.3	-0.8	Least altered basalt with thin veins
801C-46R1,106	899	1.6	13.9	11.3	13.2	0.1	7.1	0.21	2.57	0.2	47.7	2.0	0.020	-5.0	61.4	-5.0	-5.0		Least altered basalt
801C-52M1,47	933	1.8	13.7	11.5	14.4	0.1	7.4	0.27	2.85	0.2	48.5	2.3	0.014						Least altered basalt
801 SUPER	750	7.7	11.1	12.0	12.7	0.6	5.7	0.21	2.12	0.15	45.4	1.54	0.092	-6.8	72.0	-2.7	-8.4	-3.8	Composite

* CrS/ΣS corresponds to the proportion (in %) of Cr-reducible S (pyrite) relative to total S measured

Table 2: Individual $\delta^{34}S$ analysis of secondary sulfides in Hole 801C

Sample	Description	$\delta^{34}S$
801B-43R1,29 - 499.4 mbsf		
mar-1*	marcasite aggregate with minor pyrite disseminated in thick carbonate-rich vein (5mm thick)	-33.5
mar-2#1		-31.8
mar-2#2		-36.5
mar-3#1		-39.1
mar-3#2		-39.7
mar-3#3		-39.0
801C-2R3,59 - 506.4 mbsf		
py-1#1	Dissiminated pyrite grain (0.5mm) in carbonate rich vein (2mm thick)	-22.9
py-1#2		-28.5
801C-06R5,75 - 546.9 mbsf		
py-1#1	pyrite veinlet (0.5mm thick) lining a arbonate-rich vein (2mm thick), occurrence of pyrite aggregates locally	-36.5
py-1#2		-42.3
py-1#3		-43.4
801C-07R2,132 - 552.9 mbsf		
py-1#1	pyrite veinlet (0.1mm thick) lining a arbonate-rich vein (1mm thick)	-3.2
801C-09R1,32 - 563.5 mbsf		
py-1#1	polycrystalline marcasite aggregate disseminated in basalt groundmass	-28.3
py-1#2		-38.9
py-2#3	ditto, 2mm from py-1	-45.3
801C-15R4,69 - 618.3 mbsf		
py-1*	hand-picked pyrite grains from carbonate and saponite-rich vein (3mm thick)	-25.3
801C-16R4,9 - 627.5 mbsf		
py-1*	hand-picked pyrite grains from saponite-rich vein (2mm thick)	-26.3
801C-17R1,100 - 633.8 mbsf		
py-1#1	pyrite grains disseminated along fracture in basalt groundmass with minor carbonate and saponite	-41.7
py-1#2		-45.3
py-1#3		-43.6
py-2#1	ditto, 1mm from py-1 along vein	-7.4
py-3#1	ditto, 0.5mm from py-2 along vein	-7.1
py-4#1	ditto, 0.2mm from py-3 along vein	-10.8
py-4#2		-5.9
py-5#1	ditto, 1mm from py-4 along vein	-27.1
py-6#1	pyrite grain within basalt groudmass	-7.7
py-7#1	pyrite grain within basalt groudmass	-43.7
py-8#1	ditto	-8.8

Table 2 (continued)

Sample	Description	$\delta^{34}S$
801C-23R1,45 - 682.4 mbsf		
py-1*	local pyrite enrichment (polycrystalline aggregates) associated with carbonate-rich vesicules (1-3mm wide)	-32.5
py-2#1		-25.7
py-2#2		-32.1
py-2#3		-29.8
py-2#4		-23.9
801C-24R2,36 - 693.0 mbsf		
py-1*	pyrite associated with saponite-rich vein	-38.4
py-2#1	thin pyrite veinlet (<0.1mm)	-44.9
801C-27R1,50 - 720.2 mbsf		
py-1*	dissiminated pyrite grains lining non-mineralized fracture and extending 2mm within basalt groundmass	-7.0
py-2#1		-1.4
py-2#2		-3.8
py-2#3		-5.8
py-2#4		-3.7
801C-27R1,50 - 720.2 mbsf		
py-3#1	dissiminated pyrite grains within basalt groundmass	-10.4
py-3#2		-7.8
801C-37R1,83 - 814.1 mbsf		
py-1#1	pyrite grains with framboidal-like texture within porous basalt groundmass	0.2
py-1#2		-3.3
py-1#3		-8.9
py-2#1	polycrystalline pyrite aggregates within porous basalt groundmass	-2.3
py-2#2		-3.2
py-3#1	Coarse pyrite grain lining basalt vesicule	1.3
py-3#2		-0.6
py-1#8	Coarse pyrite grain lining basalt vesicule	-8.6
py-1#9		-17.2
801C-37R5,30 - 818.8 mbsf		
py-1*	dissiminated fine-grained pyrite within coarse-grained, porous basalt groundmass	-1.0
py-2#1		-4.2
801C-39R2,28 - 834.0 mbsf		
py-1#1	pyrite-rich veinlet (0.5mm thick) within fine grained basalt	-31.0
py-1#2		-33.2
py-1#3		-41.3
py-1#4		-11.4

* $\delta^{34}S$ values obtained on micro-drilled sulfide grains (gaz-source mass spectrometer)

Table 3: Multiple sulfur isotope composition of secondary sulfide in ODP Hole 801C normalized to VCDT scale

Sample	$\delta^{33}S$	$\delta^{34}S$	$\Delta^{33}S$	$\delta^{33}S^*$	$\delta^{34}S^*$	$\Delta^{33}S^*$	Description
Sample 801C-17R1,100							
#2	-20.541	-39.665	-0.114	-20.755	-40.473	0.089	
#3	-20.656	-39.886	-0.115	-20.872	-40.703	0.090	polycrystalline pyrite grain dissiminated along
#4	-20.418	-39.422	-0.116	-20.629	-40.220	0.084	fracture in basalt groundmass with minor
#5	-21.529	-41.521	-0.146	-21.764	-42.408	0.076	carbonate and saponite
#6	-11.066	-21.385	-0.053	-11.128	-21.617	0.005	
Sample 801C-43R1.29/V							
#7	-19.178	-37.055	-0.095	-19.364	-37.759	0.082	polycrystalline marcasite aggregate with minor
#8	-17.881	-34.556	-0.085	-18.043	-35.167	0.068	pyrite dissiminated in thick carbonate-rich vein
Sample 801C-23R1,45							
#9	-13.356	-25.762	-0.089	-13.446	-26.100	-0.005	local pyrite enrichment (polycrystalline aggregates) associated with carbonate-rich vesicules (1-3mm wide)
Sample 801C-9R1,32							
#12	-11.496	-22.121	-0.104	-11.563	-22.369	-0.042	polycrystalline marcasite aggregate dissiminated in basalt groundmass

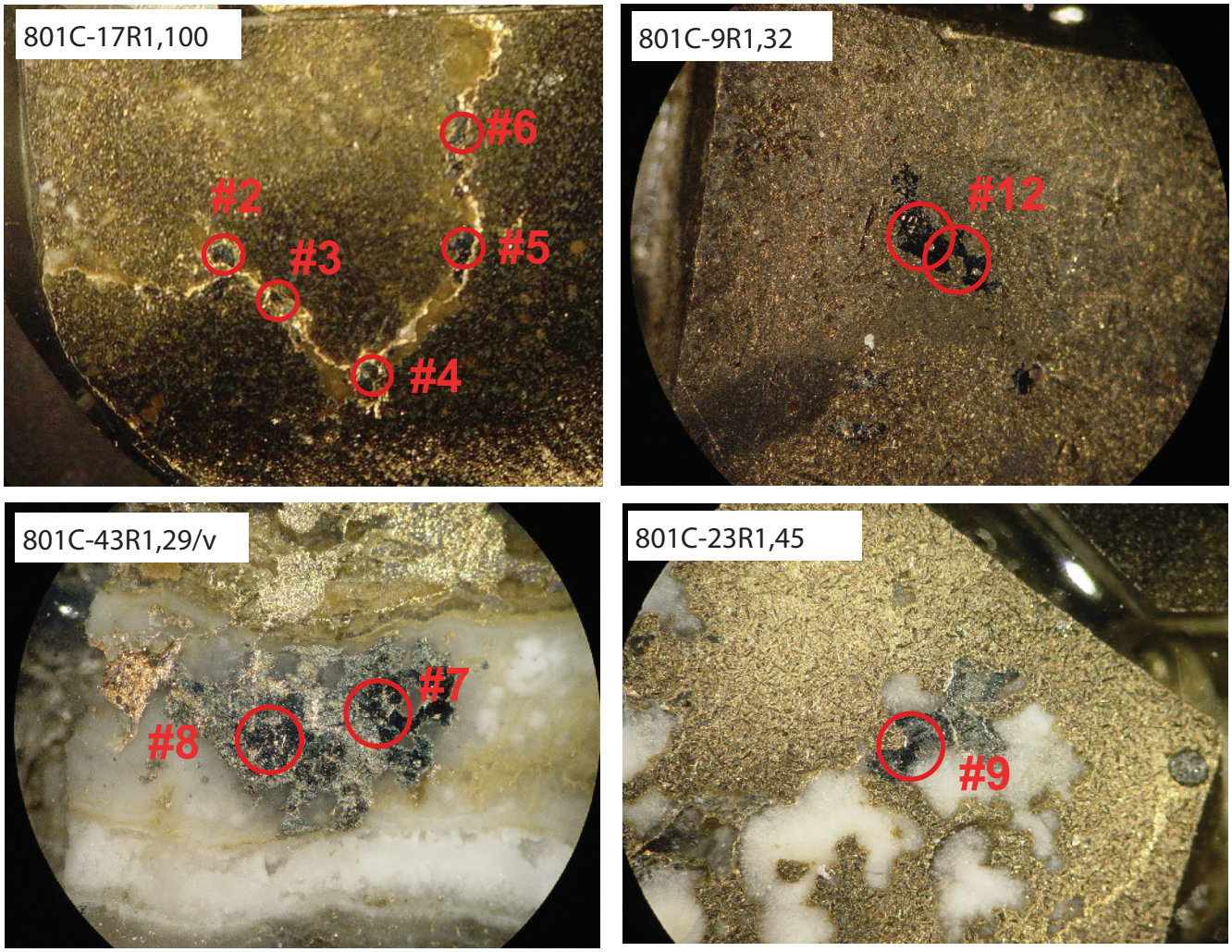

Supplementary Material : Photograph of polished section of basalt with secondary sulfides (pyrite, marcasite) analyzed for multiple S isotopes. Red circles correspond to micro-drilled areas and analysis numbers are the same as in Table 3.